

X-rays and gamma rays from active galactic nuclei

By ROLAND SVENSSON

Stockholm Observatory, S-133 36 Saltsjöbaden, Stockholm, Sweden

Various types of active galactic nuclei (AGN) are briefly discussed, with an emphasis on the theory of recent X-ray and γ -ray observations of the subclass, Seyfert 1 galaxies. The large radiation power from AGN is thought to originate from gravitational power released by matter accreting onto a supermassive black hole. The physical mechanisms responsible for the energy release and the geometry of the gaseous components are still uncertain in spite of three decades of observational and theoretical studies. The recent X-ray and γ -ray observations, however, start to provide useful constraints on the models. This kind of interpretation of the observations is possible due to theoretical developments during the last decade of radiative transfer of X-rays in both optically thick and thin media of various geometries. Particular attention is paid to various accretion disk-corona models. Recent work on exact radiative transfer in such geometries are reviewed.

1. Theoretical history

The underlying framework for almost all efforts to understand active galactic nuclei (AGN) is the accretion disk picture described in the classical papers by Novikov & Thorne (1973) and Shakura & Sunyaev (1973). This original picture was partly inspired by the extreme optical AGN luminosities. Here, effectively optically thick, rather cold matter forms a geometrically thin, differentially rotating Keplerian disk around a supermassive black hole. The differential motion causes viscous dissipation of gravitational binding energy resulting in outward transportation of angular momentum and inward transportation of matter. The dissipated energy diffuses vertically and emerges as black body radiation, mostly in the optical-UV spectral range for the case of AGN.

Observations have also been the driving force in the discovery of two other solution branches.

a) Hard X-rays from the galactic black hole candidate, Cyg X-1, as well as the discovery of strong X-ray emission from most AGN led to the need for a hot accretion disk solution. Shapiro, Lightman & Eardley (1976) (SLE) found a hot, effectively optically thin, rather geometrically thin solution branch, where the ions and the electrons are in energy balance, with the ions being heated by dissipation and cooled through Coulomb exchange, leading to ion temperatures of order 10^{11} - 10^{12} K. The efficient cooling of electrons through a variety of mechanisms above 10^9 K, leads to electron temperatures being locked around 10^9 - 10^{10} K. The SLE-solution is thermally unstable.

b) Observations of Cyg X-1 and of radio galaxies led to two independent discoveries of the third solution branch. Ichimaru (1977) developed a model to explain the soft high and hard low state of Cyg X-1. The soft high state is due to the disk being in the optically thick cold state, and the hard low state occurs when the disk develops into a very hot, optically thin state. This solution branch is similar to the SLE-solution, except that now the ions are not in local energy balance. It was found that if the ions were sufficiently hot they would not cool on an inflow time scale, but rather the ions would heat up both by adiabatic compression and viscous dissipation and would carry most of that energy with them into the black hole. Only a small fraction would be transferred to the electrons, so the efficiency of the accretion is much less

than the normal $\sim 10\%$. As the ion temperature was found to be close to virial, these disks are geometrically thick. Just as for the SLE-case above, the electrons decouple to be locked at $10^9 - 10^{10}$ K. The flows resemble the quasi-spherical dissipative flows studied by, e.g., Mészáros (1975) and Maraschi, Roasio & Treves (1982). Independently, Rees *et al.* (1982) and Phinney (1983) proposed that a similar inefficient accretion disk solution is responsible for the low nuclear luminosities in radio galaxies with large radio lobes and thus quite massive black holes. These geometrically thick disks were named *ion tori*. Rees *et al.* (1982) specified more clearly than Ichimaru (1977) the critical accretion rate above which the flow is dense enough for the ions to cool on an inflow time scale and the ion tori-branch would not exist. Further considerations of ion tori were made by Begelman, Sikora & Rees (1987). Ichimaru (1977) emphasized that his version of ion tori is thermally stable.

The ion-tori branch has been extensively studied and applied over the last two years (1995-1996) with more than 30 papers by Narayan and co-workers, Abramowicz and co-workers, as well as many others. These studies confirm and extend the original results, although some papers do not quote or recognize the original results. New terminology has been introduced based on an Eulerian viewpoint rather than a Lagrangian. Instead of the ions not cooling, it is said that the local volume is "advectively cooled" due to the ions carrying away their energy. The *ion tori* are therefore renamed as *advection-dominated disks*.

The three accretion disk branches were "unified" by Chen *et al.* (1996) and Björnsson *et al.* (1996), who determined where in parameter space the branches merges. Parallel to these developments there have been several other lines of research regarding the physics needed for realistic modelling of accretion flows. These areas include radiative processes in hot plasmas, radiation transfer in hot plasmas, radiation transfer of X-rays in cold plasma, MHD in differentially rotating gas, the origin of disk viscosity, magnetic flares, gas or MHD-simulations of flows, and so on. Some of these research lines have already merged. Here we focus on the areas most important for interpreting the high energy spectra of AGN.

While the classical rates for bremsstrahlung, cyclo/synchrotron radiation, and Compton scattering in the nonrelativistic and relativistic limits were sufficient in the early disk models, the electron temperatures of $10^9 - 10^{10}$ K indicated by both observations and theory required the calculation of transrelativistic rates of the above processes as well as for pair processes that becomes important at these temperatures. Rate calculations as well as exploring the properties of pair and energy balance in hot plasma clouds were done in the 1980s by Lightman, Svensson, Zdziarski and others. Methods to incorporate these sometimes complex hot plasma solutions into the simplest accretion disk models were developed by Björnsson & Svensson (1991, 1992). The Compton scattering kernel probably received its definite treatment in Nagirner & Poutanen (1994).

To obtain approximate spectra, the Kompaneets equation with relativistic corrections and with a simple escape probability replacing the radiative transfer is sufficient (Lightman & Zdziarski 1987). However, if one want to obtain constraints on the geometry from detailed observed spectra, then methods to obtain exact radiative transfer/Comptonization solutions in different accretion geometries must be developed. Here again, Igor Novikov had great influence as he and his group stimulated a particle physicist and expert on Monte Carlo simulations, Boris Stern, to develop a Monte Carlo code able to treat all the high energy radiative processes occurring in AGN. The first results were reported in Kardashev, Novikov & Stern (1986) and Novikov & Stern (1986), and an advanced version of the code was finally documented in Stern *et al.* (1995a). Faster methods were developed by Haardt (1993) (approximate treatment of the Compton scattering)

and Poutanen & Svensson (1996) (exact treatment) who solved the radiative transfer for each scattering order separately (the iterative scattering method). These codes are fast enough to be implemented in XSPEC, the standard X-ray spectral fitting package, and exactly computed model spectra can now be used when interpreting the observations. So far these methods have been used to study radiative transfer in two-phase media consisting of cold and hot gas with simple geometries, but they have yet to be integrated in the standard accretion disk models.

UV and X-ray observations indicate the coexistence of both cold and hot matter in AGN. Then one must be able to compute the reprocessing (both absorption, reflection, and transmission) of X-rays by the cold matter. The first approximate considerations of Compton reflection by Guilbert & Rees (1988) and White, Lightman, & Zdziarski (1988) have now led to quite accurate methods developed by Magdziarz & Zdziarski (1995) and Poutanen, Nagendra & Svensson (1996). Such Compton reflection forms an important ingredient in the radiative transfer calculations in two-phase media.

2. Observational history

The exploration of the spectra of AGN started some 30 years ago. It is mainly due to the developments in instrumental and satellite technology that we now in the 1990s start having a full broad band picture of these spectra. In 1960s groundbased observations started exploring the optical and radio properties. The advent of X-ray astronomy allowed the 2-10 keV properties to be explored in the 1970s. The theoretical modelling then consisted of connecting the radio, optical, and the X-ray data points with one or two power laws and discussing the resulting fits within nonthermal models where relativistic power law electrons generate both power law synchrotron radiation and power law Compton-scattered radiation. The infrared spectral gap was covered in the 1980s. First after the launch in April 1991 of the *Compton Gamma Ray Observatory (CGRO)* covering the gamma ray spectral range did we get a full broad band view of AGN spectra and thus reliable estimates of their total luminosities and the spectral ranges where most of the luminosity was emitted. As described in Dermer & Gehrels (1995), AGN fell into two distinct classes, the γ -loud and the γ -weak AGN. The γ -loud AGN are the luminous blazars where we are looking down into a relativistic jet emerging from the AGN. Here, the power emerges in two broad band humps, one due to nonthermal synchrotron emission peaking in the IR-optical spectral range, the second due to Compton scattering peaking in the MeV-GeV spectral range. The γ -weak AGN, on the other hand, are the less luminous Seyfert and radio galaxies (being spiral and ellipticals, respectively), where the spectra extends from radio frequencies to the soft γ -rays (100s of keV). These spectra have approximately equal power per logarithmic frequency interval, but show many spectral features, in particular, three broad band spectral peaks at infrared, UV, and hard X-ray frequencies. The fast time variability of the UV to soft γ -ray spectra indicates that this emission is "nuclear" radiation originating in the accretion flow very close to the black hole. The slowly varying broad band infrared spectral peak originates at larger distances, most likely being due to nuclear radiation being reprocessed by dust. The nuclear spectra has been studied for more than 20 years, yet little is known about the physical conditions close to the super massive black holes in AGN.

Both Seyfert (normally being radio-weak) and radio galaxies comes in two types based on optical classification. Seyfert 1 and the broad line radio galaxies show Doppler-broadened broad (up to 10 000 km/s) and narrow (up to perhaps 1000 km/s) emission lines, while the Seyfert 2 galaxies and the narrow line radio galaxies show only the narrow emission lines. The broad lines originate in fast-moving photo-ionized 10^4 K gas clouds

within 1 parsec of the central source, while the narrow lines originate in slower moving clouds at kiloparsec distances. Aspects of radio galaxies are discussed in the chapter by Malcolm Longair in this volume. Here, we will focus on the Seyfert galaxies only.

In the unified scheme for Seyfert galaxies (e.g. Antonucci 1993), we are directly viewing the central X-ray source and broad line region in Seyfert 1 galaxies, but our line-of-sight passes through an optically opaque molecular torus in Seyfert 2 galaxies obscuring both the central source and the broad line region but not the narrow line region. The photo-ionized narrow line gas lies in an ionization cone whose half-opening angle is determined by the geometry of the obscuring torus. In some Seyfert 2 galaxies we still see weak polarized broad lines being reflected by electrons in the ionization cone. In standard accretion disk scenarios for the central X-ray source, the unified models imply that our viewing angle (i.e. the angle between the disk normal and the line-of-sight) is less than the half-opening angle of the ionization cone for the case of Seyfert 1s. Half-opening angles inferred from observations are typically 30-40 degrees, which means that in Seyfert 1s we are viewing the accretion disk from directions that are closer to face-on than to edge-on.

3. X-ray and γ -ray spectra of Seyfert galaxies

The satellites (launch year and energy range in parenthesis) *ROSAT* (June 1990; 0.1-2 keV), *ASCA* (Feb 1993; 0.1-10 keV), *Ginga* (Feb 1987 - Nov 1991; 2-40 keV), *SAX* (April 1996; 0.2-200 keV), *XTE* (Dec 1995; 2-200 keV), and *CGRO* (April 1991; 50 keV-30 GeV) have allowed broad band X/ γ -ray studies of some 30 Seyfert galaxies in the 1990s. However, as AGN varies in the X-rays on time-scales down to days or even hours simultaneous measurements are necessary. Such simultaneous observations unfortunately exist for only a handful objects, but the number is increasing. The launch of *INTEGRAL* (2 keV-10 MeV) in the year 2001 will finally provide a large number of truly simultaneous X/ γ -spectra of AGN.

By combining observations in different energy bands, a picture has emerged where the overall shapes of the X-ray and γ -ray spectra of different Seyfert 1 galaxies are similar. The only Seyfert 1 galaxy for which the broad band X- and γ -ray spectrum is well determined is IC 4329A (Madejski *et al.* 1995) being the second brightest Seyfert galaxy in the 2-10 keV range. Simultaneous *ROSAT* and *CGRO* OSSE, as well as nonsimultaneous *Ginga* data are shown in Figure 1 (*left panel*). The observations were modelled by Madejski *et al.* (1995), Zdziarski *et al.* (1994), and Magdziarz & Zdziarski (1995). The spectrum consists of two components: 1) an intrinsic power law of slope $\alpha_{\text{int}} \approx 0.9$ with an exponential cutoff energy of about 300 keV (dashed curve in Fig. 1), and 2) a reflection component caused by cold reflecting matter subtending a solid angle $\sim 1 - 2\pi$ as viewed from the X-ray source (dotted curve in Fig. 1). The reflection component consists of a fluorescent Fe line at 6.4 keV and a broad peak at about 30 keV causing the overall 2-18 keV spectral slope to be considerably flatter, $\alpha_{2-18} \approx 0.7$ and the apparent cutoff energy to be smaller, ≈ 50 keV. A small column depth of neutral material about $N_{\text{H}} = 3 \times 10^{21}$ cm⁻² along the line of sight causes absorption below 2 keV.

The average X/ γ -spectrum for four Seyfert 1s using nonsimultaneous *Ginga* and OSSE data shows similar properties as the spectrum for IC 4329A (Zdziarski *et al.* 1995). The same holds for the nonsimultaneous average *EXOSAT*/OSSE spectrum for seven Seyfert 1s (Gondek *et al.* 1996).

Larger samples exist within narrower spectral ranges using a single experiment. These samples show spectra consistent with the smaller samples above. For example, 60 *Ginga* spectra of 27 Seyferts show $\alpha_{\text{int},2-18} \approx 0.95$ and the overall $\alpha_{2-18} \approx 0.73$, each having a dispersion of about 0.15 (Nandra & Pounds 1994).

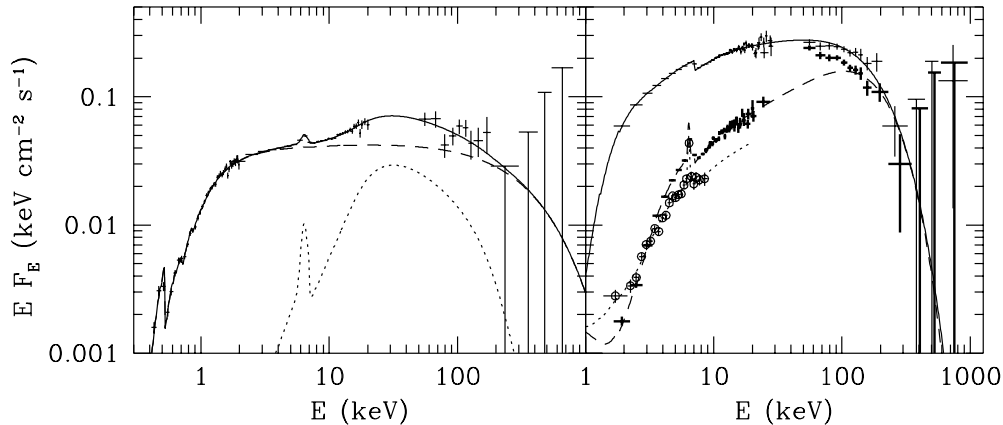


FIGURE 1. *Left panel* shows the observed broad band spectrum (*crosses*) of IC 4329A from *ROSAT*, *Ginga*, and *CGRO* OSSE (Madejski *et al.* 1995). The *dashed curve* shows the intrinsic model spectrum incident on both the cold matter and the observer, the *dotted curve* is the reflected component, and the *solid curve* is the observed sum. From Magdziarz & Zdziarski (1995). *Right panel* shows the observed broad band spectrum of NGC 4151 from *Ginga*, and *CGRO* OSSE (*crosses*) and from *EXOSAT* (*circled crosses*). The *EXOSAT* data are from April 1984, the highest and lowest *Ginga* data from May 1990 and May 1987, respectively, and the highest and lowest *CGRO* OSSE data from May and April 1993, respectively. *Solid, dashed, and dotted curves* show fits to the data using a simple thermal Comptonization model. From Zdziarski, Johnson & Magdziarz (1996).

The brightest Seyfert galaxy, the Seyfert 1.5 NGC 4151, once considered a prototype for Seyfert 1s, has now turned out to have unusual X-ray properties. Figure 1 (*right panel*) from Zdziarski, Johnson & Magdziarz (1996) shows the extreme spectral states of NGC 4151. In the 2-18 keV *Ginga*-range, the spectral index, α_{2-18} , varies in the range 0.3-0.8 instead of having the canonical Seyfert value of 0.7. The harder the spectrum is, the weaker is the 2-18 keV flux, and the spectrum seems to pivot around 100 keV. And indeed, OSSE observations during 1991-1994 show that the OSSE flux is essentially constant. NGC 4151 shows no or a smaller reflection component than normal Seyfert 1s. This causes the deduced intrinsic power law component to have a smaller cut off energy than the standard Seyfert 1, although the total OSSE spectra are indistinguishable. NGC 4151 also have a larger column depth $N_{\text{H}} \sim 10^{23} \text{ cm}^{-2}$ of absorbing gas along the line of sight compared to typical Seyfert 1s. This causes absorption below about 6 keV. Optical observations of an ionization cone indicates that we are not viewing NGC 4151 face-on but rather at a viewing angle of 65 degrees. NGC 4151 is clearly a freak object which requires special consideration to fit into the unified scheme of Seyfert galaxies. The standard interpretation is that we have a direct view of the central X-ray source, but it has also been proposed (Poutanen *et al.* 1996) that the central X-ray source is obscured and that the observed X-ray spectrum is a standard Seyfert 1 spectrum scattered by about 65 degrees into the line of sight. Compton recoil then decreases the spectral cut off energy.

The observed obscuring column depths in Seyfert 2 galaxies lies in the range $N_{\text{H}} \sim 2 \times 10^{22} - 5 \times 10^{23} \text{ cm}^{-2}$ (Smith & Done 1996). An extreme case is NGC 4945 (Done, Madejski & Smith 1996) whose broad band X-ray spectrum is shown in Figure 2. Here, the absorbing column is very large, $N_{\text{H}} \sim 4 \times 10^{24} \text{ cm}^{-2}$, causing absorption of the direct spectrum below 20 keV. Below 10 keV the spectrum is dominated by a weak component

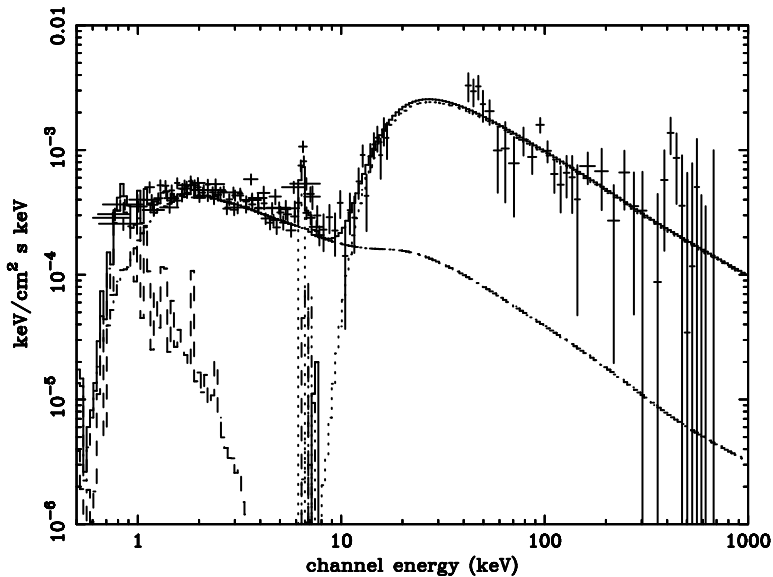


FIGURE 2. The broad band spectrum (*crosses*) of NGC 4945 from *ASCA*, *Ginga*, and *CGRO* OSSE. The *dotted curve* is the direct power law spectrum being absorbed below 20 keV by a column depth $N_{\text{H}} \sim 4 \times 10^{24} \text{ cm}^{-2}$. The *dash-dotted curve* shows the component scattered into the line-of-sight by electrons in the ionization cone. The effects of a reflection component is included. From Done, Madejski & Smith (1996).

that has been scattered into the line-of-sight by electrons in the ionization cone. Although weak in the 2-10 keV range, NGC 4945 is the second brightest known Seyfert galaxy in the sky above 50 keV. In the Seyfert 2 galaxy, NGC 1068, the absorbing column is even larger and the scattered component dominates at least up to 20 keV (Koyama *et al.* 1989).

4. Outstanding questions regarding the X-ray emitting regions in Seyfert 1 galaxies

The obvious question is of course which radiation process generates the X-ray continuum. It is commonly believed that Compton scattering by energetic electrons, either mildly relativistic thermal electrons or highly relativistic nonthermal electrons, Compton scatter soft UV-photons into the X-ray range.

Then there is the question of geometry, i.e. the spatial distribution of hot X-ray generating electrons and of cold ($T < 10^6 \text{ K}$) reflecting matter. Possible geometries include a cold slab surrounded either by plane parallel coronal slabs of hot electrons, or by coronal patches (active regions) of unknown geometries.

Finally, there is the question whether it is thermal or nonthermal electrons or both that account for the X-ray emission. This question might be answered if the spectrum above a few hundred keV was known with certainty, but the best available spectrum of the brightest typical Seyfert 1, IC 4329A, does not have sufficient signal to noise at such energies. The spectrum of IC 4329A can be fit with both thermal and nonthermal models (Zdziarski *et al.* 1994).

The nonthermal models studied in the 1980s have several attractive features (for review, see Svensson 1994). In particular, it was predicted already in 1985 (Svensson 1986)

that the pair cascades in the nonthermal models give rise to an X-ray spectrum with $\alpha_{\text{int},2-18} \approx 0.9 - 1.0$ in contradiction to the overall slope of $\alpha_{2-18} \approx 0.7$ but in agreement with the intrinsic spectral slope later found by *Ginga* (e.g. Nandra & Pounds 1994).

Due to the non-detections by COMPTEL and the high energy cutoffs indicated by OSSE, attention is now focused on the thermal models.

5. Geometry of the X-ray source

In principle, the central X-ray source could have spherical symmetry with the source of UV-photons being small cold clouds uniformly distributed throughout the X-ray source. In this case, radiation models invoking spherical symmetry would be applicable (e.g., Ghisellini & Haardt 1994, Skibo *et al.* 1995; Pietrini & Krolik 1995). In some models, the central X-ray source is quasi-spherical but the UV-source is anisotropic. Here, the X-ray source can either be a hot two-temperature SLE-accretion disk or a two-temperature ion torus. The UV-source may then be the standard cold Shakura-Sunyaev disk located beyond some transition radius. Another proposed alternative is that the disk is hot at larger radii but that in the innermost region the cooling times become sufficiently short for the disk to collapse into a cold UV-emitting disk state. The resulting anisotropy of the UV-photons breaks the spherical symmetry in both of these scenarios. Then detailed radiative transfer calculations of how the UV-photons penetrate the hot disk are required in order to determine the emerging X-ray spectrum of Comptonized UV-photons at different viewing angles. This problem has not yet been solved.

The most commonly used scenario (mainly because of its simplicity) is the two-phase disk-corona model (e.g., Haardt & Maraschi 1991, 1993) in which a hot X-ray emitting corona is located above the cold UV-emitting disk of the canonical black hole model for AGNs. The power law X-ray spectrum is generated by thermal Comptonization of the soft UV-radiation. About half of the X-rays enters and is reprocessed by the cold disk, emerging mostly as black body disk radiation in the UV. Haardt & Maraschi (1991) emphasized the coupling between the two phases due to the reprocessing, as the soft disk photons influence the cooling of the corona. They showed that nearly all power must be dissipated in the corona in order to have $\alpha_{\text{int}} \sim 0.9 - 1$. A consequence of this is that the soft disk luminosity, L_s , is of the same order as the hard X-ray luminosity, L_h . The disk-corona scenario is highly anisotropic as the UV-photons enter the corona from below only.

Observations show that L_s may be several times larger than L_h , in contradiction to the prediction of the uniform two-phase disk-corona model. This led Haardt, Maraschi, & Ghisellini (1994) to propose a patchy disk-corona model, where the corona consists of several localized active regions on the surface of the disk. Internal disk dissipation results in UV-radiation that leaves the disk without entering the active regions, thus enhancing the observed L_s relative to L_h . The patchy corona model is also highly anisotropic as the UV-radiation enters the active regions from below and through the sides. The active regions could also be elevated above the disk.

The full radiative transfer and Comptonization problem in these geometries has recently been solved (Haardt & Maraschi 1993, Stern *et al.* 1995b, Poutanen & Svensson 1996). We now turn to discuss the methods and the results.

6. Radiative transfer/Comptonization

Two different methods have been used to solve the full radiative transfer/Comptonization problem in mildly relativistic thermal plasmas accounting for energy and pair balance as well as reprocessing by the cold disk (including angular anisotropy and Klein-Nishina effects).

The first method is based on the Non-Linear Monte Carlo (NLMC) method developed by Stern (1985, 1988) and described in detail in Stern *et al.* (1995a). The Monte Carlo particles (particles and photons) make up the background so the Monte Carlo particles can interact with themselves (e.g. photon-photon pair production) causing nonlinearity. Any geometry can be treated including 2D and 3D geometries, but calculations so far (Stern *et al.* 1995b) have been limited to coronal slabs (1D) or active regions (2D) in the shape of hemispheres or spheres at different elevations above the cold disc. Another advantage is the possibility to divide the region into several zones in order to study the inhomogeneous distributions of, e.g., temperature and pair density. The drawback is that each run takes a few hours on a Sun IPX.

The second method is based on the iterative scattering method (ISM), where the radiative transfer is exactly solved for each scattering order separately (e.g. Sunyaev & Titarchuk 1985, Haardt 1994). The code and its testing are briefly described in Poutanen and Svensson (1996, see also Poutanen 1994; Poutanen & Vilhu 1993). It was shown that the results of the NLMC and the ISM code are in excellent agreement. The ISM code is a 1D code but it can also treat quasi-2D radiative transfer in cylinders/pill boxes and hemispheres. The full Compton scattering matrix is used allowing to solve polarized radiative transfer in thermal relativistic plasmas. Fully angular dependent, polarized Compton reflection is implemented using a Green's matrix (Poutanen, Nagendra & Svensson 1996). The advantage of the ISM code is that it takes 10 minutes or less on a Sun IPX.

7. The Comptonization solution

The two codes have been used to study radiative transfer/Comptonization in pure pair coronae in energy and pair balance. For coronae of a given geometry and in energy balance, there exists a unique $T_e - \tau_T$ relation, where T_e is the volume-averaged coronal temperature and τ_T is a characteristic Thomson scattering optical depth of the coronal region. For slabs, τ_T is the vertical Thomson scattering optical depth. For hemispheres and for spheres, the radial τ_T is averaged over 2π solid angle for hemispheres, and 4π solid angle for spheres.

In Figure 3a, this relation is shown for different geometries. The results for slabs are shown by *rectangles*, for hemispheres located on the disk surface by *hemispheres*, for surface spheres located on the disk surface by *underlined spheres*, and for spheres located at heights, $0.5h$, $1h$, and $2h$, by *spheres*, *diamonds*, and *triangles*, respectively (h is the radius of the sphere). The results for active regions are connected by *dotted* curves. For comparison we also show the slab results from Stern *et al.* 1995b using the ISM code (*dashed curve*). Each curve is characterized by an almost constant generalized Kompaneets parameter, $y \equiv \tau_T(1 + \tau_T)(4\Theta + 16\Theta^2)$, where $\Theta \equiv kT_e/m_e c^2$, and where $y \sim 0.49$ for slabs, ~ 2.0 for hemispheres, and $\sim 2.3, 3.7, 5.9$, and 7.8 for the spheres. The larger the soft photon starvation (i.e. the fewer the number of reprocessed soft photons reentering the coronal region), the larger is y . There is very good agreement between the slab results from the NLMC and the ISM codes, which tests the accuracy of both codes and methods.

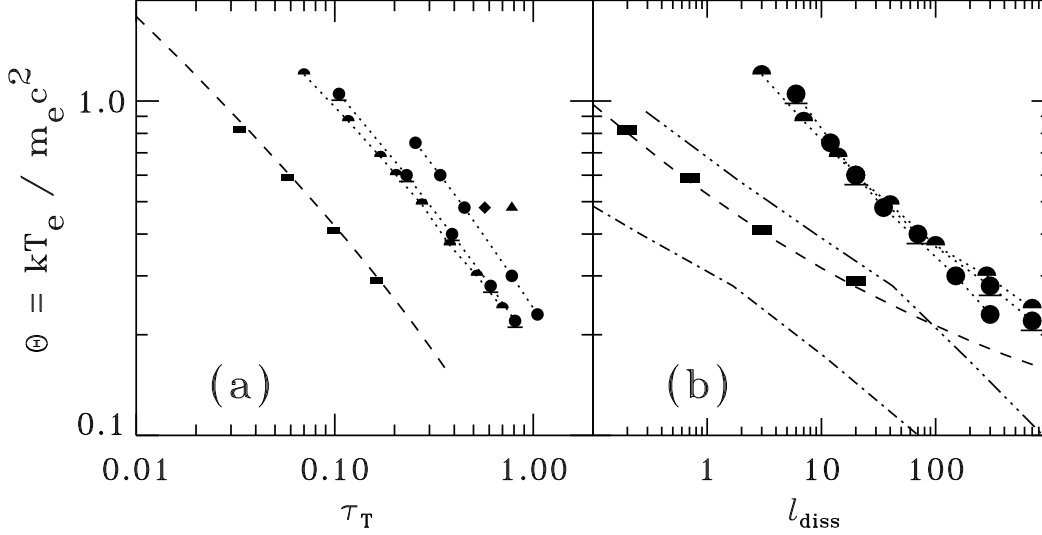


FIGURE 3. Dimensionless volume-averaged temperature, $\Theta \equiv kT_e/m_e c^2$, vs. Thomson scattering optical depth, τ_T , in panel (a), and vs. dissipation compactness, $\ell_{\text{diss}} \equiv (L_{\text{diss}}/h)(\sigma_T/m_e c^3)$ in panel (b), for a steady X-ray emitting plasma region in pair and energy balance on or above a cold disk surface of temperature, $kT_{\text{bb}} = 5$ eV. The plasma Compton scatters reprocessed soft black body photons from the cold disk surface. *Solid rectangles* and *dashed curve* show results from NLMC code and ISM code, respectively, for the case of a plane-parallel slab corona. Results using the NLMC code for individual active pair regions are shown for *hemispheres* located on the disk surface; surface spheres also located on the surface (*underlined spheres*); spheres located at a height of $0.5h$ (*spheres*), $1h$ (*diamond*), and $2h$ (*triangle*), where h is the radius of the sphere. The results for each type of active region are connected by *dotted curves*. The *dash-dotted* and *dash-dot-dot-dotted* curves in panel (b) show the critical compactness as function of Θ above which thermalization by Moller and Bhabha scattering is not achieved for the cases of pair slabs and surface spheres, respectively. From Stern *et al.* (1997).

8. Pair balance and the compactness

Solving the pair balance for the combinations of (Θ, τ_T) obtained in § 7 gives a unique dissipation compactness, ℓ_{diss} (see Ghisellini & Haardt 1994 for a discussion). Here, the local dissipation compactness, $\ell_{\text{diss}} \equiv (L_{\text{diss}}/h)(\sigma_T/m_e c^3)$, characterizes the dissipation with L_{diss} being the power providing uniform heating in a cubic volume of size h in the case of a slab of height h , or in the whole volume in the case of an active region of size h . The Figure 3b shows the Θ vs. ℓ_{diss} relation obtained with the NLMC code for different geometries and for $kT_{\text{bb}} = 5$ eV. The slab results with the ISM codes are also shown by the dashed curve. The parameter space to the right of respective curve is forbidden as pair balance cannot be achieved, and the parameter space to the left would contain solutions where the background coronal plasma dominates over the pairs, i.e. “pair free” solutions (e.g. Svensson 1984, HM93). Note that the pair temperatures are locked in the range $\Theta \sim 0.15 - 1$ (80 – 500 keV) for the considered compactnesses. The pairs thus act as a “thermostat” (e.g., Svensson 1984)

From Figure 3b we find that at a given Θ the active regions have a larger ℓ_{diss} than the slabs. This is due to the longer escape times in slabs. In a local cubic volume in slabs, the four vertical surfaces act effectively as “reflecting” surfaces increasing the radiation

energy density in the volume as compared to the active regions where the radiation escapes freely through the surface of the volume.

9. Thermalization

The question arises whether the electrons can thermalize or not for the conditions, Θ , τ_T , and ℓ_{diss} , in Figure 3. Energy exchange and thermalization through Moller ($e^\pm e^\pm$) and Bhabha ($e^+ e^-$) scattering compete with various loss mechanisms, with Compton losses being the most important for our conditions. The thermalization is slowest and the Compton losses largest for the higher energy particles in the Maxwellian tail. Ghisellini, Haardt & Fabian (1993) compared average Maxwellian time scales to find the conditions when thermalization is not achieved. Instead we use the detailed simulations by Dermer & Liang (1989) (their Fig. 8) to find the critical compactness above which the deviation at the Maxwellian mean energy is more than a factor $e \approx 2.7$. The *dash-dotted* and *dash-dot-dot-dotted* curves in Figure 3b show this critical compactness for slabs and for surface spheres, respectively. In agreement with Ghisellini, Haardt & Fabian (1993), we find that Moller and Bhabha scattering cannot compete with Compton losses in our pair slabs and active regions. On the other hand, Ghisellini, Guilbert & Svensson (1988) and Ghisellini & Svensson (1990) found that cyclo/synchrotron self-absorption acts as a very efficient thermalizing mechanism as long as the magnetic energy density dominates the radiation energy density, a condition expected in the corona and in the magnetic flares on the surface of accretion disks.

10. Anisotropy effects

Figure 4 shows the “face-on” emerging spectrum for a hemisphere with $\ell_{\text{diss}} = 20$ and $kT_{\text{bb}} = 5$ eV with the reflected component subtracted. The *solid curve* is the sum of the reprocessed soft black body spectrum and the Comptonized spectrum. The “face-on” spectrum is averaged over viewing angles $0.6 < \cos\theta < 1$. The numbered *dotted curves* show spectral profiles of the different scattering orders. As noted by Haardt (1993) and HM93, the first scattering order is significantly reduced in face-on directions due to anisotropic Compton scattering when Θ is mildly relativistic. This deficiency at low energies causes an *anisotropy break* close to the peak of the second scattering order. Below the anisotropy break, the spectrum is a power law with an *anisotropy slope*, α_{aniso} , that is harder than the standard *isotropy slope*, α_{iso} , above the break. It is the standard isotropy slope, α_{iso} , that has been fitted with several analytical expressions that are functions of Θ and τ_T (e.g., Zdziarski 1985, Titarchuk 1994). “Edge-on” spectra have a much weaker reflection component and no anisotropy break.

11. Spectra from active pair regions: hemispheres

Figure 5 shows emerging “face-one” and “edge-on” spectra from hemispheres at different ℓ_{diss} for $kT_{\text{bb}} = 5$ eV. We have $\alpha_{\text{aniso}} \approx 0.77$ while $\alpha_{\text{iso}} \approx 1.09$. The anisotropy break is therefore about 0.3. The anisotropy break moves through the 2-18 keV range for $\ell_{\text{diss}} \approx 10$ -100, and thus α_{2-18} is smaller than unity for ℓ_{diss} less than 100. At this low kT_{bb} the first Compton order hardly extends into the 2-18 keV range and there is little discreteness effect on the behavior of α_{2-18} .

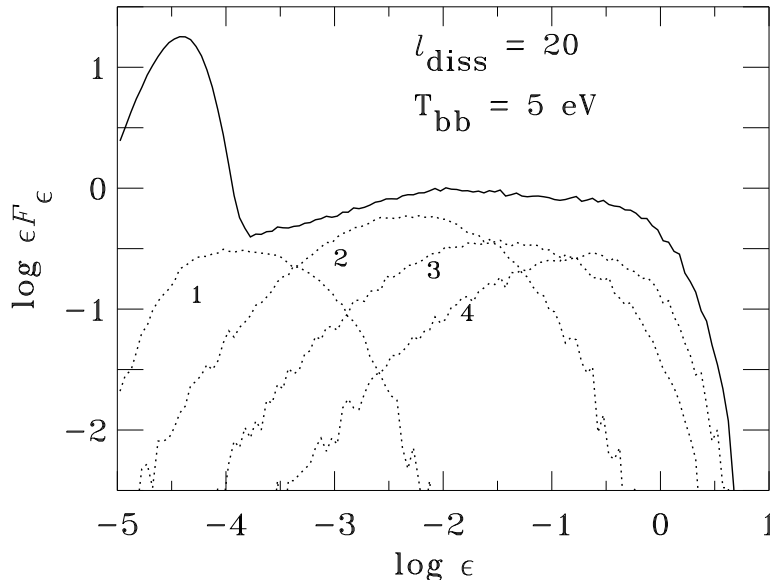


FIGURE 4. Emerging spectrum, ϵF_ϵ , where F_ϵ is the energy flux (arbitrary units) and $\epsilon \equiv h\nu/m_e c^2$ from hemisphere with compactness, $\ell_{\text{diss}} = 20$, and cold disk temperature, $kT_{\text{bb}} = 5$ eV. The spectrum is averaged over viewing angles $0.6 < \cos\theta < 1$. The *solid curve* shows the sum of the Comptonized spectrum from the hemisphere and the reprocessed black body spectrum (the reflection component is not included). The numbered *dotted curves* show the different scattering orders. Note that the first scattering order is significantly reduced due to anisotropic Compton scattering. This deficiency causes an *anisotropy break* close to the peak of the second scattering order. Below the anisotropy break, the spectrum is a power law with an *anisotropy slope* that is harder than the standard *isotropy slope* above the break. From Stern *et al.* (1997).

12. Diagnostics Using Compactness and *Ginga* Slopes

The least square overall spectral slope, α_{2-18} , for the 2-18 keV range were determined and are displayed in Figure 6 as a function of the dissipation compactness, ℓ_{diss} , for different geometries. The *right panel* of Figure 6 shows the observed distribution of α_{2-18} for *Ginga* spectra from 27 Seyfert galaxies (Nandra & Pounds 1994). The *crosses* represent 17 Seyfert galaxies that have both been observed by *Ginga* and have known estimates of their X-ray time variability (and thus lower limits of their compactnesses). The true crosses may lie to the right of the plotted ones.

One sees that the observations are more consistent with active surface regions (such as hemispheres or surface spheres) than with slabs. Active regions produce spectra covering the *observed ranges* of α_{2-18} ($\approx 0.4 - 0.9$) and cutoff energies ($\sim 2kT_e$) for the *observed range* of compactnesses.

13. Conclusions

Have we been able to throw some light upon the outstanding questions discussed in § 4?

Regarding the radiative transfer/Comptonization, the progress has been rapid and it is now possible to use full radiative transfer simulations when fitting X-ray observations, e.g. with XSPEC, at least for the simplest geometries (e.g., Poutanen *et al.* 1996 for the case of NGC 4151). As anisotropic effects are very important, i.e. as spectral shapes

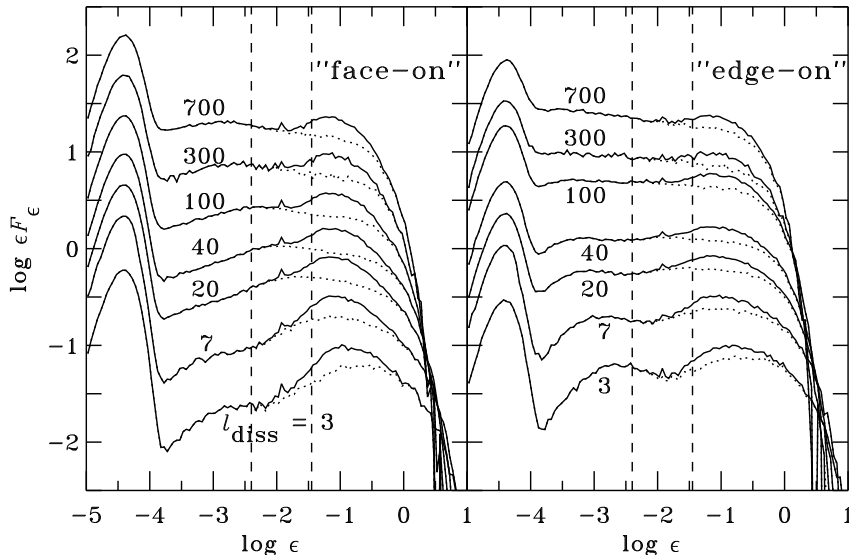


FIGURE 5. Emerging “face-on” and “edge-on” spectra, ϵF_ϵ , where F_ϵ is the energy flux (arbitrary units) and $\epsilon \equiv h\nu/m_e c^2$, from hemispheres of different compactnesses, ℓ_{diss} and for cold disk temperature, $kT_{\text{bb}} = 5$ eV. The “face-on” spectra are averaged over viewing angles $0.6 < \cos\theta < 1$, and the “edge-on” spectra over viewing angles $0 < \cos\theta < 0.5$. The *solid curves* show the total spectrum which is the sum of the Comptonized spectrum from the hemisphere itself (*dotted curves*), the reprocessed black body spectrum, and the reflection component. Vertical *dashed lines* show the 2-18 keV spectral range. The anisotropy break in the face-on spectra moves to lower photon energies as ℓ_{diss} increases. From Stern et al. (1995b, 1997).

depend strongly on viewing angle, it will be possible to set constraints on the viewing angle. The ISM code also gives detailed predictions for the spectral X/ γ -ray polarization, which may provide crucial constraints once observations become available.

The spectra also depend on the geometry of the coronal regions, so observed spectra can be used as diagnostics of the geometry. Presently, it seems that active regions are favoured over homogeneous slab coronae.

There is still no answer to the question whether the radiating electrons (and positrons) are thermal or nonthermal. High quality spectra above 200 keV are needed, and the question may not be settled before the launch of *INTEGRAL* in the year 2001.

The author acknowledges support from the Swedish Natural Science Research Council. He thanks Juri Poutanen, Marek Sikora, and Boris Stern for numerous valuable discussions. Boris Stern’s research visits at the Stockholm Observatory were financed by the Swedish Institute, the Swedish Royal Academy of Sciences, and by a NORDITA Nordic project grant.

REFERENCES

- ANTONUCCI, R. 1993 Unified models for active galactic nuclei and quasars. *Ann. Rev. Astr. Astroph.* **31**, 473–521.
- BEGELMAN, M. C., SIKORA, M. & REES, M. J. 1987 Thermal and dynamical effects of pair production on two temperature accretion flows. *Astrophys. J.* **313**, 689–698.

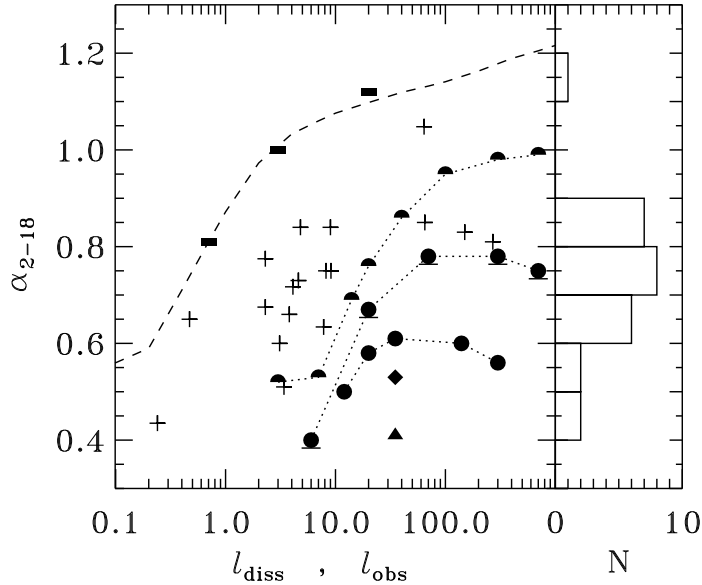


FIGURE 6. Overall spectral intensity index, α_{2-18} , least square fitted to the model spectra in the 2-18 keV range vs. the dissipation compactness, l_{diss} . Same notation as in Fig. 3. The spectra from the NLMC code were averaged over viewing angles $0.6 < \cos \theta < 1.0$ before determining α_{2-18} with least square fitting. For the ISM code, face-on spectra (at $\cos \theta = 0.887$) were used. The right panel shows the observed distribution of α_{2-18} for *Ginga* spectra from 27 Seyfert galaxies (Nandra & Pounds 1994). The crosses represent 17 Seyfert galaxies that have both been observed by *Ginga* and have known estimates of their X-ray time variability, Δt , and thus of the observed compactness, $l_{\text{obs}} \equiv (L_{\text{obs}}/c\Delta t)(\sigma_{\text{T}}/m_e c^3)$. From Stern *et al.* (1995b, 1997).

- BJÖRNSSON, G. & SVENSSON, R. 1991 A recipe for making hot accretion disks. *Astrophys. J. Letters* **371**, L69–L72.
- BJÖRNSSON, G. & SVENSSON, R. 1992 Hot pair dominated accretion disks. *Astrophys. J.*, **394**, 500–514.
- BJÖRNSSON, G., CHEN, X., ABRAMOWICZ, M. A., & LASOTA, J. P. 1996 Hot accretion disks revisited. *Astroph. J.*, in press.
- CHEN, X., ABRAMOWICZ, M. A., LASOTA, J. P., NARAYAN, R. & YI, I. 1996 Unified description of accretion flow around black holes. *Astroph. J. Letters* **443**, L61–L64.
- DERMER, C. D. & GEHRELS, N. 1995 Two classes of gamma-ray emitting active galactic nuclei. *Astrophys. J.* **447**, 103–120.
- DERMER, C. D. & LIANG, E. P. 1989 Electron thermalization and heating in relativistic plasmas. *Astrophys. J.* **339**, 512–528.
- DONE, C., MADEJSKI, G. M. & SMITH, D. A. 1996 NGC 4945: The brightest Seyfert 2 galaxy at 100 keV. *Astrophys. J. Letters* **463**, L63–L66.
- GHISELLINI, G. & HAARDT, F. 1994 On thermal Comptonization in e^{\pm} pair plasmas. *Astroph. J. Letters* / **429**, L53–L56.
- GHISELLINI, G. & SVENSSON, R. 1990 Synchrotron self-absorption as a thermalizing mechanism. in *Physical Processes in Hot Cosmic Plasmas* (eds. W. Brinkmann, A. C. Fabian & F. Giovannelli) pp. 395–400. Kluwer.
- GHISELLINI, G., HAARDT, F. & FABIAN, A. C. 1993 On reacceleration, pairs and the high energy spectrum of AGN and Galactic black hole candidates. *Monthly Not. Roy. Astr. Soc.* **263**, L9–L12.
- GHISELLINI, G., GUILBERT, P. W. & SVENSSON, R. 1988 The synchrotron boiler. *Astrophysical Journal Letters* **335**, L5–L8.

- GONDEK, D., *et al.* 1996 The average X-ray/gamma-ray spectrum of radio-quiet Seyfert 1s. *Monthly Not. Roy. Astr. Soc.*, in press.
- GUILBERT, P. W. & REES, M. J. 1988 ‘Cold’ material in non-thermal sources. *Monthly Not. Roy. Astr. Soc.* **233**, 475–484.
- HAARDT, F. 1993 Anisotropic Comptonization in thermal plasmas: spectral distribution in plane parallel geometry. *Astrophys. J.* **413**, 680–693.
- HAARDT, F. 1994 High Energy Processes in Seyfert Galaxies. PhD dissertation, SISSA, Trieste.
- HAARDT, F. & MARASCHI, L. 1991 A two-phase model for the X-ray emission from Seyfert galaxies. *Astrophys. J. Letters* **380**, L51–L54.
- HAARDT, F. & MARASCHI, L. 1993 X-ray spectra from two-phase accretion disks. *Astrophys. J.* **413**, 507–517.
- HAARDT, F., MARASCHI, L. & GHISELLINI, G. 1994 A model for the X-ray and UV emission from Seyfert galaxies and galactic black holes. *Astrophys. J. Letters* **432**, L95–L99.
- ICHIMARU, S. 1977 Bimodal behavior of accretion disks: theory and application to Cyg X-1 transitions. *Astrophys. J.* **214**, 840–855.
- KARDASHEV, N. S., NOVIKOV, I. D. & STERN, B. E. 1986 An electron-positron cauldron and the formation of the hard radiation of quasars and AGN. In *IAU Symp. 119: Quasars* (ed. G. Swarup & V. K. Kapahi) pp. 383–393. D. Reidel.
- KOYAMA, K. *et al.* 1989 An intense iron line in NGC 1068. *Publ. Astron. Soc. Japan* **41**, 731–737.
- LIGHTMAN, A. P. & ZDZIARSKI, A. A. 1987 Pair production and Compton scattering in compact sources and comparison to observations of active galactic nuclei. *Astrophys. J.* **319**, 643–661.
- MADEJSKI, G. M. *et al.* 1995 Joint *ROSAT-COMPTON GRO* observations of the X-ray-bright Seyfert galaxy IC 4329A. *Astrophys. J.* **438**, 672–679.
- MAGDZIARZ, P. & ZDZIARSKI, A. A. 1995 Angle-dependent Compton reflection of X-rays and gamma-rays. *Monthly Not. Roy. Astron. Soc.* **273**, 837–848.
- MARASCHI, L., ROASIO, R. & TREVES, A. 1982 The effect of multiple Compton scattering on the temperature and emission spectra of accreting black holes. *Astrophys. J.* **253**, 312–317.
- MÉSZÁROZ, P. 1975 Radiation from spherical accretion onto black holes. *Astr. Astroph.* **44**, 59–68.
- NAGIRNER, D. J. & POUTANEN, J. 1993 Compton scattering of polarized light: scattering matrix for isotropic electron gas. *Astr. Astroph.* **275**, 325–336.
- NAGIRNER, D. J. & POUTANEN, J. 1994 Single Compton scattering. *Astrophys. Space Phys.* **9**, 1–47.
- NANDRA, K. & POUNDS, K. A. 1994 *Ginga* observations of the X-ray spectra of Seyfert galaxies. *Monthly Not. Roy. Astron. Soc.* **268**, 405–429.
- NOVIKOV, I. D. & STERN, B. E. 1986 A possible mechanism of the formation of the hard spectrum of active galactic nuclei. In *Structure and Evolution of Active Galactic Nuclei* (ed. G. Gluricin *et al.*) pp. 149–171. D. Reidel.
- NOVIKOV, I. D. & THORNE, K. S. 1973 Astrophysics of black holes. In *Black Holes, Les Houches* (ed. C. De Witt & B. DeWitt) pp. 343–450. Gordon & Breach.
- PHINNEY, E. S. 1983 A theory of radio sources. PhD dissertation, University of Cambridge.
- PIETRINI, P. & KROLIK, J. H. 1995 The inverse Compton thermostat in hot plasmas near accreting black holes. *Astrophys. J.* **447**, 526–544.
- POUTANEN, J. 1994 Compton scattering matrix for relativistic Maxwellian electron distribution. *J. Quant. Spectrosc. Rad. Transfer* **51**, 813–822.
- POUTANEN, J. 1994 Compton scattering of polarized light in active galactic nuclei and X-ray binaries. PhD dissertation, University of Helsinki.
- POUTANEN, J. & SVENSSON, R. 1996 The two-phase pair corona model for active galactic nuclei and X-ray binaries: How to obtain exact solutions. *Astrophys. J.* in press.
- POUTANEN, J. & VILHU, O. 1993 Compton scattering of polarized light in two-phase accretion

- discs. *Astr. Astroph.* **275**, 337–344.
- POUTANEN, J., NAGENDRA, K. N. & SVENSSON, R. 1996 Green's matrix for Compton reflection of polarized radiation from cold matter. *Monthly Not. Roy. Astron. Soc.*, in press.
- POUTANEN, J., SIKORA, M., BEGELMAN, M. C. & MAGDZIARZ, P. 1996 The Compton mirror in NGC 4151. *Astrophys. J. Letters* **465**, L107–L110.
- REES, M. J., BEGELMAN, M. C., BLANDFORD, R. D. & PHINNEY, E. S. 1982 Ion-supported tori and the origin of radio jets. *Nature* **295**, 17–21.
- SHAKURA, N. I. & SUNYAEV, R. A. 1973 Black holes in binary systems. Observational appearance. *Astr. Astroph.* **24**, 337–355.
- SHAPIRO, S. L., LIGHTMAN, A. P. & EARDLEY D. N. 1976 A two-temperature accretion disk model for Cygnus X-1: structure and spectrum. *Astrophys. J.* **204**, 187–199.
- SKIBO, J. G., DERMER, C. D., RAMATY, R. & MCKINLEY, J. M. 1995 Thermal Comptonization in mildly relativistic pair plasmas. *Astrophys. J.* **446**, 86–100.
- SMITH, D. A. & DONE, C. 1996 Unified theories of AGN: A hard X-ray sample of Seyfert 2 galaxies. *Monthly Not. Roy. Astron. Soc.*, in press.
- STERN, B. E. 1985 On the possibility of efficient production of electron-positron pairs near pulsars and accreting black holes. *Sov. Astr.* **29**, 306–313.
- STERN, B. E. 1988 Nonthermal pair production in active galactic nuclei: A detailed radiation transfer model. *Nordita/88-51 A*, preprint.
- STERN, B. E., BEGELMAN, M. C., SIKORA, M. & SVENSSON, R. 1995a A large-particle Monte Carlo code for simulating non-linear high-energy processes near compact objects. *Monthly Not. Roy. Astron. Soc.* **272**, 291–307.
- STERN, B. E., POUTANEN, J., SVENSSON, R., SIKORA, M. & BEGELMAN M. C. 1995b On the geometry of the X-ray emitting region in Seyfert galaxies. *Astrophys. J. Letters* **449**, L13–L17.
- STERN, B. E. *et al.* 1997, in preparation.
- SUNYAEV, R. A. & TITARCHUK, L. G. 1985 Comptonization of low-frequency radiation in accretion disks: angular distribution and polarized hard radiation. *Astr. Astroph.* **143**, 374–388.
- SVENSSON, R. 1984 Steady mildly relativistic thermal plasmas: processes and properties. *Monthly Not. Roy. Astron. Soc.* **209**, 175–208.
- SVENSSON, R. 1986 Physical processes in active galactic nuclei. In *IAU Coll. 89: Radiation Hydrodynamics in Stars and Compact Objects* (ed. D. Mihalas & K-H. Winkler), pp. 325–345. Springer.
- SVENSSON, R. 1994 The nonthermal pair model for the X-ray and gamma-ray spectra from active galactic nuclei. *Astrophys. J. Suppl.* **92**, 585–592.
- TITARCHUK L. 1994 Generalized Comptonization models and applications to recent high-energy observations. *Astrophys. J.* **434**, 570–586.
- WHITE, T. R., LIGHTMAN, A. P., ZDZIARSKI, A. A. 1988 Compton reflection of gamma rays by cold electrons. *Astrophys. J.* **331**, 939–948.
- ZDZIARSKI, A. A. 1985 Power-law X-ray and gamma-ray emission from relativistic thermal plasmas. *Astrophys. J.* **289**, 514–525.
- ZDZIARSKI, A. A. *et al.* 1994 Physical processes in the X-ray/gamma-ray source of IC 4329A. *Monthly Not. Roy. Astron. Soc.* **269**, L55–L60.
- ZDZIARSKI, A. A., JOHNSON, W. N. & MAGDZIARZ, P. 1996 Broad-band gamma-ray and X-ray spectra of NGC 4151 and their implications for physical processes and geometry. *Monthly Not. Roy. Astron. Soc.*, in press.
- ZDZIARSKI, A. A., JOHNSON, W. N., DONE, C., SMITH, D. & McNARON-BROWN, K. 1995 The average X-ray/gamma-ray spectra of Seyfert galaxies from *Ginga* and OSSE and the origin of the cosmic X-ray background. *Astrophys. J. Letters* **438**, L63–L66.